Journal of
Marine Science and Engineering

MDPI

Article

Reliability Assessment for Integrated Seaport Energy System Considering Multiple Thermal Inertia

Tiankai Yang [1,*], Zhenzhong Sun [1], Yongliang Liang [2] and Lichuan Liu [1]

[1] College of Marine Electrical Engineering, Dalian Maritime University, Dalian 116026, China; sunzz001@dlmu.edu.cn (Z.S.); llc1987@dlmu.edu.cn (L.L.)
[2] School of Electrical Engineering, Shandong University, Jinan 250100, China; liangyl@sdu.edu.cn
* Correspondence: tiankai900@dlmu.edu.cn

Abstract: With the rapid development of global trade, a large number of goods and resources are imported and exported via seaports. Multiple thermal loads and renewable energy merge into seaports, making the energy supply and demand structure increasingly complex. The traditional seaport becomes an integrated seaport energy system (ISES). Due to the complicated energy interaction of cooling, heating, electricity, and gas subsystems, the ISES urgently require reliable and secure operation. Hence, this paper proposes a new reliability assessment method for the ISES that considers thermal inertia. Firstly, the operational structure of the ISES is established considering multi-energy coupling relationships. Then, a two-stage optimal load curtailment model is constructed with multiple thermal inertias. In addition, the reliability assessment method for the ISES is proposed based on the sequential Monte Carlo simulation method. Simulations are presented to verify the effectiveness of the proposed method.

Keywords: integrated seaport energy system; reliability assessment; thermal inertia; multi-energy coupling relationship; sequential Monte Carlo simulation

Citation: Yang, T.; Sun, Z.; Liang, Y.; Liu, L. Reliability Assessment for Integrated Seaport Energy System Considering Multiple Thermal Inertia. *J. Mar. Sci. Eng.* **2024**, *12*, 606. https://doi.org/10.3390/jmse12040606

Academic Editors: Rabiul Islam and Sidum Adumene

Received: 15 February 2024
Revised: 28 March 2024
Accepted: 29 March 2024
Published: 31 March 2024

1. Introduction

As vital transportation hubs bridging cities and oceans, seaports are inherently energy-intensive areas [1]. They not only cater to the power demands of shore power, logistics, and industrial production but also face seasonal heating and cooling loads [2]. This substantial energy consumption brings significant challenges for low-carbon operations. The seaport microgrid's current single-energy supply structure needs to be revised to meet the escalating energy demands and urgently requires transformation. Since multi-energy complementarity and cascaded energy utilization can effectively enhance energy utilization efficiency and mitigate carbon emissions [3], energy conversion devices like CCHP units are increasingly deployed in seaports. Consequently, the integrated seaport energy system (ISES) is gradually evolving [4]. The practice has demonstrated that the ISES is a crucial strategy to satisfy diverse energy needs and enhance operational reliability, surpassing the capabilities of seaport microgrids [5].

However, energy supply reliability severely limits the development of the ISES [6,7]. Compared to traditional microgrids, the ISES exhibits notable disparities in structure and operational mechanisms. With the high penetration of energy conversion devices, the coupling relationships of electricity, heating, and cooling systems are ever close, and the operation state after failure becomes complicated. For example, the malfunction of CCHP units might trigger cascading failures across electric and thermal systems; the outage in the electric system would lead to a shortage of heating or cooling services. Hence, the coupling of multiple energy subsystems makes the energy structure of the ISES more complex, rendering traditional reliability indicators insufficiently comprehensive [8]. Thus, it is necessary to research reliability assessment methods for the ISES and provide valuable guidance for system planning and operation [9].

This paper provides an overview of the reliability evaluation of integrated energy systems from three aspects: the component outage model, system model and evaluation, and fault state analysis [10,11].

The reliability assessment relies heavily on the component outage model. In regional integrated energy systems, components are categorized into two main types, independent and coupling components, based on their functional capabilities [12]. Independent components, including lines, pipelines, and compressors, maintain distinct energy attributes for each subsystem, ensuring the uninterrupted energy flow. Coupling components, including the EB, GT, CHP, and CCHP, are the core devices responsible for energy conversion, bridging different energy systems, and facilitating seamless integration [13]. In [14], the two-state probability model of "run-shutdown" is established for coupling devices in electric–thermal integrated energy systems, including CHP, the GT, and the AC, and provides a valuable framework for reliability analysis. However, it overlooks the crucial influence of thermal–electric coupling on the operational state of units. Similarly, the three-state outage model employed in [15] for CCHP units based on the Markov method also fails to capture this crucial aspect.

Based on component failure characteristics, simple systems can be modeled using reliability block diagrams, fault tree analysis, Markov state space, and analytic methods for evaluation [16–18]. In [19], the energy hub represents the intricate relationships between energy input, conversion, storage, and output. Due to the characteristics of randomness in source, load, multi-energy coupling, and energy storage, sequential Monte Carlo methods are commonly adopted for system evaluation [20]. In [21], the operation model of the electrical–thermal system is established, considering the intricate relationship between gas pipeline flow and node pressure. In [22], considering the physical characteristics of natural gas density, temperature, and flow velocity, a dynamic model is established to characterize the short-term flow process of the natural gas network. However, simulating failure-free states significantly increases the computational scale, seriously impacting the efficiency and convergence of sequential simulation methods [23].

With the fault components and system state, fault state analysis is conducted to evaluate the consequences of faults. The typical analysis methods need to establish an optimal load-shedding model to minimize load reduction considering operational constraints [24]. Specifically, since the ISES integrates a great diversity of energy sources, it has multiple response characteristics after system failure, which should be considered during the analysis. In [25], load transfer is achieved through distribution network interconnection lines during system faults, and a thermal load-shedding model considering security constraints is established. In [26], an optimization load-shedding model is established with photovoltaic power, combined heat and power units, and electric boilers as control variables. In [27], further reliability improvements can be achieved by fully utilizing the short-term dynamic thermal characteristics. In [28], a two-stage optimization scheduling model is developed for large-scale comprehensive energy systems.

Although existing research has proven that the economy and flexibility of the integrated energy system can be improved considering thermal inertia, there are still the following problems to be solved:

(1) The multi-time scale issues pose significant challenges to the reliability assessment of the ISES. Electric services immediately degrade when failure occurs, while the thermal demand can be satisfied for a period owing to the gradual degradation of temperatures. Hence, the impact of the coexistence of heterogeneous energy should be considered.

(2) Given the significant differences in operating characteristics among various energy systems within the ISES, it is imperative to establish suitable reliability indexes that accurately reflect the reliability level of each system based on unique energy characteristics.

Therefore, this paper proposes a novel reliability assessment method based on the sequential Monte Carlo simulation method for the ISES. Firstly, the energy supply and demand structure of the ISES is introduced to describe the coupling relationship of electricity, gas, heating, and cooling systems. Secondly, considering multiple thermal inertia, a two-stage optimal model is established to minimize the load curtailment. Thirdly, the reliability indexes are modified for the ISES, and a sequential Monte-Carlo-based method is constructed to evaluate the reliability. The remaining contents are organized as follows. Section 2 provides the basic structure of the ISES and coupled energy relationships. Section 3 presents a two-stage load curtailment method. Section 4 proposes reliability indexes considering thermal inertia and constructs a Monte Carlo sequential-simulation-based reliability assessment method. Section 5 validates the effectiveness of the proposed method. Section 6 concludes.

2. Operation Structure of ISES

As an effective measure for integrating various energy sources and different energy systems, the integrated energy system has been widely applied and developed in many regions to improve energy efficiency and reduce pollution emissions. Based on the architecture of the IES, this paper considers the characteristics of energy supply and demand in seaports. It proposes the basic structure of the ISES, as depicted in Figure 1. Here, the ISES includes the cooling chain, thermal loads, and electric/heating storages and centrally schedules all energy supply, conversion, and storage devices. The corresponding abbreviations and notations are depicted in Table 1, Table 2, and Table 3, respectively.

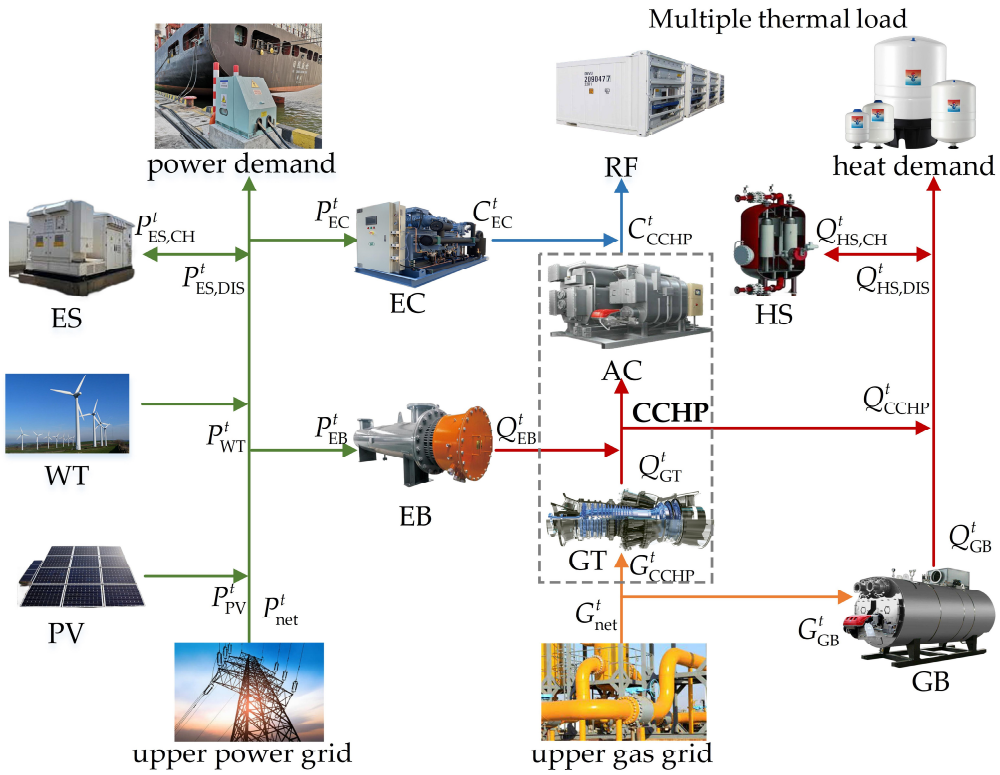

Figure 1. The framework of ISES.

Table 1. Abbreviations.

Abbreviations	Full Name	Abbreviations	Full Name
ISES	Integrated seaport energy system	HS	Heating storage
IES	Integrated energy system	GB	Gas boiler
CCHP	Combined cooling, heating, and power	EB	Electric boiler
CHP	Combined heating and power	EENS	Expectation of energy not supply
GT	Gas turbine	LOLE	Loss of load expectation
AC	Absorption chiller	TSELE	Total shutdown energy loss expectation
EC	Electrical chiller	SAI	Service availability index
ES	Electrical storage	RF	Reefer container

Table 2. Notation for parameters.

Operation Parameters	
λ, μ	Failure and repair rates of each component
R_{GT}	Ramp rate of GT (kW/h)
R_{GB}	Ramp rate of GB (kW/h)
R_{EB}	Ramp rate of EB (kW/h)
ξ_E^t, ξ_G^t	Purchase prices of electricity and gas (¥/kWh)
ξ_P, ξ_Q, ξ_C	Load curtailment penalty coefficients of power, heating, and cooling, respectively (¥/kWh)
H^g	The calorific value of natural gas (MWh/m^3)
Power parameters	
$COP_{\mathrm{GT}}^{\mathrm{e}}$	Power generation efficiency of GT
$\eta_{\mathrm{ES,CH}}$, $\eta_{\mathrm{ES,DIS}}$	Charging and discharging efficiency of ES, respectively
Heating parameters	
$COP_{\mathrm{GT}}^{\mathrm{h}}$, $COP_{\mathrm{GB}}^{\mathrm{h}}$, $COP_{\mathrm{EB}}^{\mathrm{h}}$	Thermal efficiency of GT, GB, and EB, respectively
$COP_{\mathrm{GT}}^{\mathrm{h,loss}}$	Heating loss efficiency of GT
R	Thermal conductivity of hot water tank (W/°C)
C	Heating capacity of hot water tank (J/°C)
$T_{\mathrm{tank}}^{\mathrm{ex}}$	Initial desired temperatures of hot water tank (°C)
$\eta_{\mathrm{HS,CH}}$, $\eta_{\mathrm{HS,DIS}}$	Charging and discharging efficiency of HS, respectively
Cooling parameters	
COP_{AC}^{c}, COP_{EC}^{c}	Cooling efficiency of AC and EC, respectively
k	Heating transfer coefficient of RF (w/(m^2·°C))
m	Cargo weight of RF (kg)
C_p	Specific heating capacity of RF (kJ/(kg·°C))
A	Surface area of RF (m^2)
$T_{\mathrm{RF}}^{\mathrm{ex}}$	Initial desired temperatures of RF (°C)

Table 3. Notation for variables.

Decision Variables	
P_{CCHP}^t	Power production of CCHP (kW)
P_{WT}^t, P_{PV}^t	Output power of wind turbine and solar panel, respectively (kW)
P_{EB}^t, P_{EC}^t	Power consumption of EB and EC, respectively (kW)
$P_{\mathrm{ES,CH}}^t$, $P_{\mathrm{ES,DIS}}^t$	Charged and discharged power of ES, respectively (kW)
P_{net}^t, G_{net}^t	Input power of the upper power grid and gas grid, respectively (kW)
P_{d}^t, Q_{d}^t, C_{d}^t	Entire electric, heating, and cooling loads of ISES, respectively (kW)
P_{cut}^t, Q_{cut}^t, C_{cut}^t	Load curtailment of power, heating, and cooling, respectively (kW)
Q_{GT}^t	Recoverable heating power of GT (kW)
Q_{GB}^t, Q_{EB}^t, Q_{CCHP}^t	Output heating power of GB, EB, and CCHP, respectively (kW)
$Q_{\mathrm{HS,CH}}^t$, $Q_{\mathrm{HS,DIS}}^t$	Charged and discharged heating power of HS, respectively (kW)
C_{CCHP}^t, C_{EC}^t	Cooling production of CCHP and EC, respectively (kW)

Table 3. *Cont.*

Decision Variables	
G^t_{CCHP}, G^t_{GB}	Intake power of CCHP and GB, respectively (kW)
V^t_{GT}	Gas consumption rate of GT (m^3/h)
T^t_{RF}	Temperature of RF (°C)
T^t_a	Ambient temperature (°C)
T^t_{tank}	Water temperature of hot water tank (°C)
E^t_{ES}, E^t_{HS}	Storage capabilities of ES and HS, respectively (kWh)
t_{TTR}	Time to repair (h)
t_{TTF}	Time to fault (h)
State variables	
$x^t_{\mathrm{ES,CH}}$, $x^t_{\mathrm{ES,DIS}}$	Binary status markers of ES for charging and discharging states, respectively
$x^t_{\mathrm{HS,CH}}$, $x^t_{\mathrm{HS,DIS}}$	Binary status markers of HS for charging and discharging states, respectively
x^t_{Pcut}, x^t_{Qcut}, x^t_{Ccut}	Curtailment indexes for electric, heating, and cooling loads, respectively

2.1. Constraints for the Cooling Chain

The RF in the cooling chain applies the CCHP for cooling [29]. The operation constraints of the cooling chain include conversion and capacity constraints, shown as follows:

$$C^t_{\mathrm{EC}} = COP^{\mathrm{C}}_{\mathrm{EC}} \cdot P^t_{\mathrm{EC}} \tag{1}$$

$$C^t_{\mathrm{CCHP}} = COP^{\mathrm{c}}_{\mathrm{AC}} \cdot (Q^t_{\mathrm{GT}} - Q^t_{\mathrm{CCHP}}) \tag{2}$$

$$Q^t_{\mathrm{GT}} = (1 - COP^{\mathrm{e}}_{\mathrm{GT}} - COP^{\mathrm{h,loss}}_{\mathrm{GT}}) \cdot G^t_{\mathrm{CCHP}} \tag{3}$$

$$G^t_{\mathrm{CCHP}} = V^t_{\mathrm{GT}} \cdot H^g \tag{4}$$

$$0 \le P^t_{\mathrm{EC}} \le P^M_{\mathrm{EC}} \tag{5}$$

$$0 \le G^t_{\mathrm{CCHP}} \le G^M_{\mathrm{CCHP}} \tag{6}$$

$$R^m_{\mathrm{GT}} \le \frac{G^{t+\Delta t}_{\mathrm{CCHP}} - G^t_{\mathrm{CCHP}}}{\Delta t} \le R^M_{\mathrm{GT}} \tag{7}$$

where the superscripts M and m represent the upper and lower limits of variables, respectively; Δt is the scheduling time interval.

During the refrigeration, the temperature variation model of the RF is presented as follows [30]:

$$T^{t+\Delta t}_{\mathrm{RF}} = T^t_{\mathrm{RF}} - \frac{(C^t_{\mathrm{EC}} + C^t_{\mathrm{CCHP}})\Delta t}{mC_p} \tag{8}$$

When cold load curtailment occurs, the temperature of the RF increases with the prolonged load curtailment time, resulting in the operation state transition, and the expression is depicted as follows [31]:

$$T^{t+\Delta t}_{\mathrm{RF}} = T^t_{\mathrm{RF}} + \left[T^t_a - T^t_{\mathrm{RF}}\right]\left(1 - e^{\frac{-A \cdot k \cdot \Delta t}{10^3 \cdot m \cdot C_p}}\right) \tag{9}$$

where T^t_a is the ambient temperature at time t; A is the surface area of the RF; k is the heating transfer coefficient of contents in the RF.

Furthermore, the constraint of the temperature of the RF is shown as follows:

$$T^{\mathrm{ex}}_{\mathrm{RF}} \le T^t_{\mathrm{RF}} \le T^M_{\mathrm{RF}} \tag{10}$$

For the temperature variation curve of the RF shown in Figure 2a, the cooling load is cut at $t = 0$ and supplied at t_2. Meanwhile, the comparisons of cooling load curtailment considering and ignoring the thermal inertia are shown in Figure 2b. We can see that T^t_{RF} violates the upper limit at t_1, and satisfies the constraints again at t_3. In other words, due to thermal inertia, the cooling load curtailment does not immediately vary with changes in the energy supply state. Therefore, the reliability assessment with the thermal inertia of the RF is more suitable for the actual requirements.

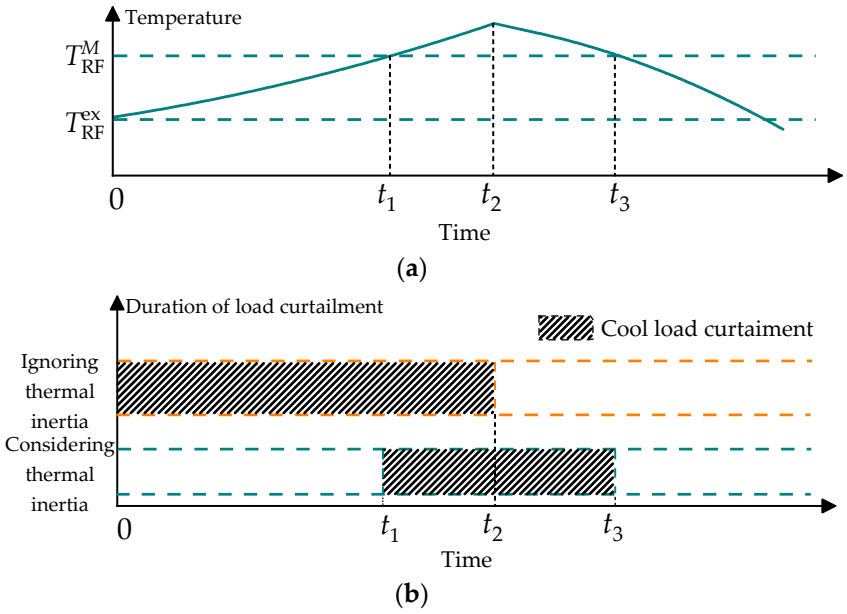

Figure 2. Thermal inertia diagram of RF. (**a**) The temperature variation curve of RF; (**b**) the cool load curtailment in ISES.

2.2. Constraints for the Heating Load

The heating load in the ISES is set as the hot water tank, and the linear energy balance method is employed to model the temperature variation of the tank, which is expressed as follows [32]:

$$T^{t+\Delta t}_{\mathrm{tank}} = T^t_{\mathrm{tank}} + \frac{1}{C}\left[-R(T^t_{\mathrm{tank}} - T^t_a) - Q^t_{\mathrm{cut}}\right] \cdot \Delta t \tag{11}$$

Furthermore, the constraint of the temperature is shown as follows:

$$T^m_{\mathrm{tank}} \le T^t_{\mathrm{tank}} \le T^{\mathrm{ex}}_{\mathrm{tank}} \tag{12}$$

For the temperature variation curve of the hot tank shown in Figure 3a, the heating load is cut at $t = 0$ and supplied at t_2. Meanwhile, the comparisons of heating load curtailment considering and ignoring the thermal inertia are shown in Figure 3b. We see that T^t_{tank} violates the lower limit at t_1 and satisfies the constraints again at t_3. In other words, due to thermal inertia, the heating load curtailment does not immediately vary with changes in the energy supply state. Therefore, the reliability assessment with the thermal inertia of the hot water tank is more suitable for the actual requirements.

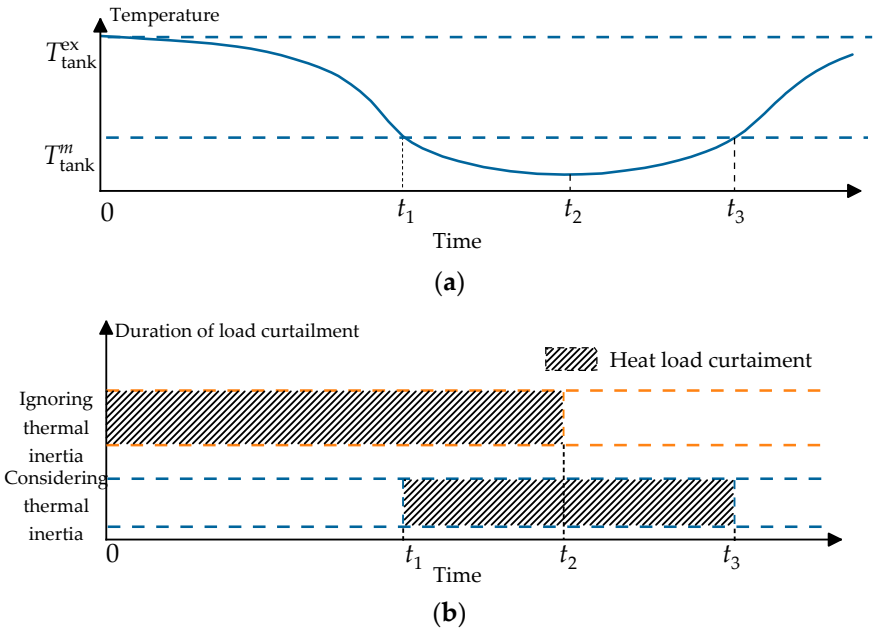

Figure 3. Thermal inertia diagram of tank. (**a**) The temperature variation curve of hot water tank; (**b**) the heat load curtailment in ISES.

2.3. Constraints for the Energy Conversion Device

The energy conversion devices of the ISES include CCHP, the EB, and the GB. Their output models are shown as follows [29]:

$$P^t_{\mathrm{CCHP}} = COP^e_{\mathrm{GT}} \cdot G^t_{\mathrm{CCHP}} \tag{13}$$

$$Q^t_{\mathrm{EB}} = COP^{\mathrm{h}}_{\mathrm{EB}} \cdot P^t_{\mathrm{EB}} \tag{14}$$

$$Q^t_{\mathrm{GB}} = COP^{\mathrm{h}}_{\mathrm{GB}} \cdot G^t_{\mathrm{GB}} \tag{15}$$

Furthermore, the operation constraints of CCHP, the EB, and the GB are shown as follows:

$$0 \le P^t_{\mathrm{EB}} \le P^M_{\mathrm{EB}} \tag{16}$$

$$R^m_{\mathrm{EB}} \le \frac{P^{t+\Delta t}_{\mathrm{EB}} - P^t_{\mathrm{EB}}}{\Delta t} \le R^M_{\mathrm{EB}} \tag{17}$$

$$0 \le G^t_{\mathrm{GB}} \le G^M_{\mathrm{GB}} \tag{18}$$

$$R^m_{\mathrm{GB}} \le \frac{G^{t+\Delta t}_{\mathrm{GB}} - G^t_{\mathrm{GB}}}{\Delta t} \le R^M_{\mathrm{GB}} \tag{19}$$

2.4. Constraints for the Electric and Heating Storage

The constraints for the ES and HS are shown as follows [33]:

$$E^{t+\Delta t}_{\mathrm{ES}} = E^t_{\mathrm{ES}} + \left[P^{t+\Delta t}_{\mathrm{ES,CH}} \cdot \eta_{\mathrm{ES,CH}} - \frac{P^{t+\Delta t}_{\mathrm{ES,DIS}}}{\eta_{\mathrm{ES,DIS}}} \right] \cdot \Delta t \tag{20}$$

$$E^{t+\Delta t}_{\mathrm{HS}} = E^t_{\mathrm{HS}} + \left[Q^{t+\Delta t}_{\mathrm{HS,CH}} \cdot \eta_{\mathrm{HS,CH}} - \frac{Q^{t+\Delta t}_{\mathrm{HS,DIS}}}{\eta_{\mathrm{HS,DIS}}} \right] \cdot \Delta t \tag{21}$$

Furthermore, the operation constraints of ES and HS are shown as follows:

$$E^m_{\mathrm{ES}} \le E^t_{\mathrm{ES}} \le E^M_{\mathrm{ES}} \tag{22}$$

$$0 \le P^t_{\mathrm{ES,CH}} \le P^M_{\mathrm{ES,CH}} \cdot x^t_{\mathrm{ES,CH}} \tag{23}$$

$$0 \le P^t_{\mathrm{ES,DIS}} \le P^M_{\mathrm{ES,DIS}} \cdot x^t_{\mathrm{ES,DIS}} \tag{24}$$

$$0 \le x^t_{\mathrm{ES,CH}} + x^t_{\mathrm{ES,DIS}} \le 1 \tag{25}$$

$$E^m_{\mathrm{HS}} \le E^t_{\mathrm{HS}} \le E^M_{\mathrm{HS}} \tag{26}$$

$$0 \le Q^t_{\mathrm{HS,CH}} \le Q^M_{\mathrm{HS,CH}} \cdot x^t_{\mathrm{HS,CH}} \tag{27}$$

$$0 \le Q^t_{\mathrm{HS,DIS}} \le Q^M_{\mathrm{HS,DIS}} \cdot x^t_{\mathrm{HS,DIS}} \tag{28}$$

$$0 \le x^t_{\mathrm{HS,CH}} + x^t_{\mathrm{HS,DIS}} \le 1 \tag{29}$$

In addition, considering that the energy storages for HS and ES should remain balanced within a scheduling period T, the following constraints need to be satisfied:

$$E^0_{\mathrm{ES}} = E^T_{\mathrm{ES}} \tag{30}$$

$$E^0_{\mathrm{HS}} = E^T_{\mathrm{HS}} \tag{31}$$

3. Two-Stage Optimal Load Curtailment Model for ISES

In this section, the assessment procedure considers the scheduling of failure-free and fault states, and a two-stage optimal load curtailment model is established for the reliability assessment of the ISES. In the first stage, the objective is to obtain the operation state when failures occur. In the second stage, the load curtailment model is established for assessment.

3.1. First Stage: Optimization for ISES in the Failure-Free State

The first stage aims to obtain the initial state of the ISES when the faults occur at time t_f. The following objective function is established to minimize the operation costs of the failure-free state.

$$\min F = \sum_{t=1}^{t_f-\Delta t} (\xi^t_E P^t_{\mathrm{net}} + \xi^t_G G^t_{\mathrm{net}})\Delta t \tag{32}$$

The energy balance constraints to be satisfied in the ISES are as follows:

$$P^t_{\mathrm{CCHP}} + P^t_{\mathrm{net}} + P^t_{\mathrm{WT}} + P^t_{\mathrm{PV}} = P^t_{\mathrm{ES,CH}} - P^t_{\mathrm{ES,DIS}} + P^t_{\mathrm{EB}} + P^t_{\mathrm{d}} + P^t_{\mathrm{EC}} \tag{33}$$

$$Q^t_{\mathrm{CCHP}} + Q^t_{\mathrm{GB}} + Q^t_{\mathrm{EB}} = Q^t_{\mathrm{HS,CH}} - Q^t_{\mathrm{HS,DIS}} + Q^t_{\mathrm{d}} \tag{34}$$

$$C^t_{\mathrm{CCHP}} + C^t_{\mathrm{EC}} = C^t_{\mathrm{d}} \tag{35}$$

$$G^t_{\mathrm{CCHP}} + G^t_{\mathrm{GB}} = G^t_{\mathrm{net}} \tag{36}$$

Additionally, the network constraints of the power and gas grids are considered as follows:

$$0 \le P^t_{\mathrm{net}} \le P^M_{\mathrm{net}} \tag{37}$$

$$0 \le G^t_{\mathrm{net}} \le G^M_{\mathrm{net}} \tag{38}$$

Meanwhile, the constraints (1)–(31) for CCHP must also be considered.

After the optimization in the first stage, $G^{t_f}_{\mathrm{CCHP}}$, $G^{t_f}_{\mathrm{GB}}$, $P^{t_f}_{\mathrm{EB}}$, $E^{t_f}_{\mathrm{ES}}$, and $E^{t_f}_{\mathrm{HS}}$ at the failure time t_f are obtained to prepare for subsequent assessment.

3.2. Second Stage: Optimization for ISES in the Fault State

During the recovery period, it is possible to minimize load curtailment by dispatching distributed generators and energy conversion devices. Therefore, this paper considers the inertial effects of thermal loads, sets the outputs of distributed generators and energy conversion devices as decision variables, and establishes an optimal load curtailment

model for the ISES. Considering the multiple load curtailment costs during the failures, the objective is shown as follows:

$$\min F = \sum_{t=t_f}^{t_f+t_i-\Delta t} (\xi_E^t P_{\text{net}}^t + \xi_G^t G_{\text{net}}^t)\Delta t + \sum_{t=t_f}^{t_f+t_i-\Delta t} (\xi_P P_{\text{cut}}^t + \xi_Q Q_{\text{cut}}^t + \xi_C C_{\text{cut}}^t)\Delta t \tag{39}$$

where t_i is the fault duration of the ith fault.

With the variables obtained from the first stage, the electric, heating, and cooling power balance constraints are modified as follows:

$$P_{\text{GT}}^t + P_{\text{net}}^t + P_{\text{WT}}^t + P_{\text{PV}}^t = P_{\text{ES,CH}}^t - P_{\text{ES,DIS}}^t + P_{\text{EB}}^t + P_{\text{d}}^t - P_{\text{cut}}^t + P_{\text{EC}}^t \tag{40}$$

$$Q_{\text{GT}}^t + Q_{\text{GB}}^t + Q_{\text{EB}}^t = Q_{\text{HS,CH}}^t - Q_{\text{HS,DIS}}^t + Q_{\text{d}}^t - Q_{\text{cut}}^t \tag{41}$$

$$C_{\text{AC}}^t + C_{\text{EC}}^t = C_{\text{d}}^t - C_{\text{cut}}^t \tag{42}$$

$$0 \le P_{\text{cut}}^t \le P_{\text{d}}^t \tag{43}$$

$$0 \le Q_{\text{cut}}^t \le Q_{\text{d}}^t \tag{44}$$

$$0 \le C_{\text{cut}}^t \le C_{\text{d}}^t \tag{45}$$

Meanwhile, the constraints (1)–(31) and (37)–(38) must also be considered.

4. Reliability Assessment Process Based on Sequential Monte Carlo

4.1. Reliability Indexes Considering Multiple Thermal Inertia in ISES

In this section, the expectation of energy not supply (EENS), the loss of load expectation (LOLE), and the total shutdown energy loss expectation (TSELE) are modified considering thermal inertia and utilized to evaluate the reliability of the ISES.

4.1.1. EENS

According to the definition of EENS in the power grid, EENS for the heating and cooling system is defined as the average expectation of the curtailed heating and cooling energy, as shown below.

$$\text{EENS}_{\text{Y}} = \frac{\sum_{t=1}^{8760N} Y_{\text{cut}}^t x_{\text{Ycut}}^t}{N}, Y \in \{P, Q, C\} \tag{46}$$

where EENS_P, EENS_Q, and EENS_C are EENS for the electric, heating, and cooling loads, respectively; N is the number of years of Monte Carlo simulation; x_{Pcut}^t, x_{Qcut}^t, and x_{Ccut}^t can be expressed as follows:

$$x_{\text{Pcut}}^t = \begin{cases} 0, & P_{\text{cut}}^t = 0 \\ 1, & P_{\text{cut}}^t \ne 0 \end{cases}, \; x_{\text{Qcut}}^t = \begin{cases} 0, & T_{\tan\text{k}}^t \ge T_{\tan\text{k}}^m \\ 1, & T_{\tan\text{k}}^t < T_{\tan\text{k}}^m \end{cases}, \; x_{\text{Ccut}}^t = \begin{cases} 0, & T_{\text{RF}}^t \le T_{\text{RF}}^M \\ 1, & T_{\text{RF}}^t > T_{\text{RF}}^M \end{cases} \tag{47}$$

Significantly, when the temperature of the heating and cooling system meets the constraints after failure, the heating and cooling load curtailment does not affect the reliability of ISES.

4.1.2. LOLE

LOLE is defined as the average energy shortage time expectation of load, as shown below.

$$\text{LOLE}_Y = \frac{\sum_{t=1}^{8760N} x_{Y\text{cut}}^t}{N}, Y \in \{P, Q, C\} \tag{48}$$

where $LOLE_P$, $LOLE_Q$, and $LOLE_C$ are LOLE for electrical, heating, and cooling loads, respectively.

4.1.3. TSELE

TSELE represents the expected economic loss caused by the annual interruption of loads. The expression of TSELE for the ISES is as follows:

$$\mathrm{TSELE} = \frac{\sum_{t=1}^{8760N} \sum_{Y \in \{P,Q,C\}} \xi_Y Y_{\mathrm{cut}}^t x_{Y\mathrm{cut}}^t}{N} \tag{49}$$

4.2. Monte Carlo Sequential-Simulation-Based Reliability Assessment

The basic idea of sequential Monte Carlo simulation is to establish a chronological transition process between failure-free and fault states and analyze each state to obtain evaluation indexes [34]. Here, the duration of the failure-free and fault states is sampled as follows [35]:

$$\begin{cases} t_{\mathrm{TTF}} = -\frac{1}{\lambda} \ln R_1 \\ t_{\mathrm{TTR}} = -\frac{1}{\mu} \ln R_2 \end{cases} \tag{50}$$

where R_1 and R_2 are the random numbers subject to the uniform distribution [0, 1], respectively. λ and μ are the failure and recovery rates of each component, which can be obtained as follows:

$$\begin{cases} \lambda = 1/\bar{t}_{\mathrm{TTF}} \\ \mu = 1/\bar{t}_{\mathrm{TTR}} \end{cases} \tag{51}$$

where $\bar{t}_{\mathrm{TTF}}$ and $\bar{t}_{\mathrm{TTR}}$ are the mean duration time of the failure-free and fault states, respectively.

Then, the Monte Carlo sequential-simulation-based reliability assessment method is illustrated in Figure 4, and the specific steps are as follows.

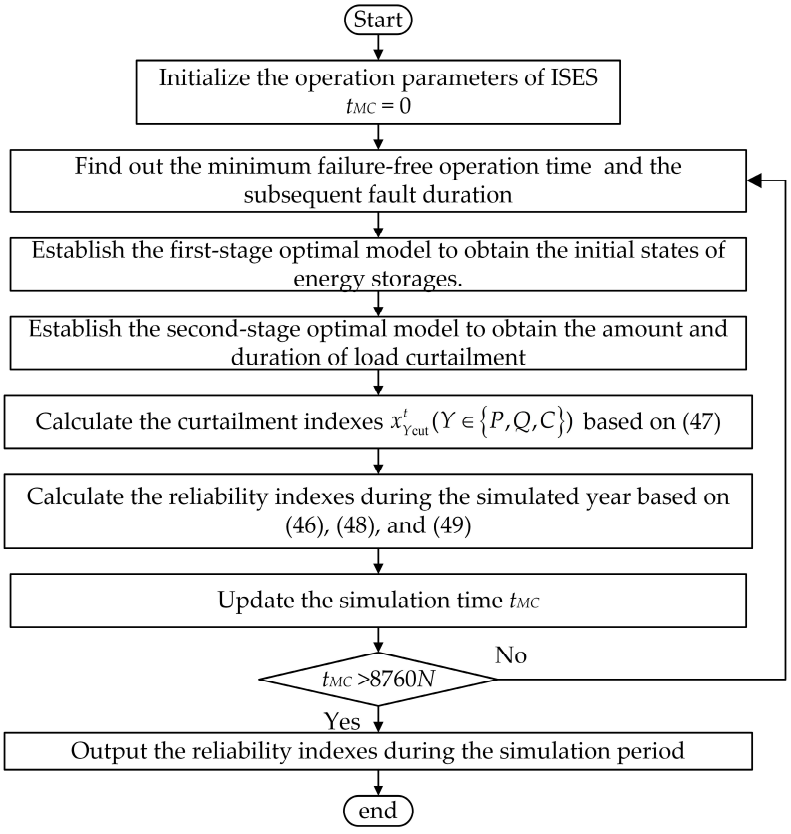

Figure 4. The reliability assessment process of ISES.

Step 1: Initialize the operation parameters of the ISES, including the topologies of electric, heating, and cooling systems, the output curves of the wind and PV generation, and the demand curves of electric, heating, and cooling loads. Set the simulation time $t_{MC} = 0$.

Step 2: According to the failure rate, the failure-free operation times of n components in the ISES can be generated as t_{TTF1}, t_{TTF2},..., t_{TTFn}. Find out the minimum failure-free operation time t^m_{TTF} and the subsequent fault duration t^m_{TTR}.

Step 3: $t_f = t_{MC} + t^m_{TTF}$. Establish the optimal model at the first stage to obtain $G^{t_f}_{CCHP}$, $G^{t_f}_{GB}$, $P^{t_f}_{EB}$, $E^{t_f}_{ES}$, and $E^{t_f}_{HS}$.

Step 4: Establish the second-stage optimal model for the fault state during the t^m_{TTR} period, and calculate the curtailment indexes $x^t_{Ycut}(Y \in \{P, Q, C\})$ based on (47).

Step 5: Calculate the average of the reliability indexes based on (46), (48), and (49).

Step 6: Update Monte Carlo simulation time $t_{MC} = t_{MC} + t^m_{TTF} + t^m_{TTR}$. If

$$t_{MC} > 8760N \tag{52}$$

output the reliability indexes; otherwise, go to step 2.

5. Simulations

5.1. Description of ISES

The ISES with electrical, gas, electrical, heating, and cooling systems as an example for simulation, and its parameters, are shown in Tables 4 and 5 [36,37]. Monte Carlo sequential simulation is utilized to evaluate the reliability of the ISES, with a maximum simulation period of 1000 years, and the power flow balance is simulated at a unified 1 h interval. Meanwhile, the electricity purchase price is 0.83 CNY/kWh at peak hours, 0.49 CNY/kWh at failure-free hours, and 0.17 CNY/kWh at valley hours. The gas purchase price is 3 CNY/m^3. The unit prices for heating and cooling energy are 0.1 CNY/kWh and 0.63 CNY/kWh. In addition, the predicted multi-energy loads of ISES and output of WT and PV are illustrated in Figure 5.

Table 4. Operation parameters of devices in ISES.

Parameter	Value	Parameter	Value	Parameter	Value
COP^{e}_{GT}	0.3	ξ_Q/(¥/kWh)	7	P^M_{net}/kW	200
$COP^{h,loss}_{GT}$	0.1	ξ_C/(¥/kWh)	8	G^M_{net}/kW	200
COP^{h}_{GT}	0.6	C/(J/°C)	4.2×10^7	G^M_{GT}/kW	100
COP^{c}_{AC}	1.2	R/(W/°C)	0.9	G^M_{GB}/kW	160
COP^{h}_{GB}	0.85	A/m^2	73.56	R^M_{GT}/(kW/h)	30
COP^{h}_{EB}	0.95	k/(W/(m^2·°C))	0.4	R^m_{GT}/(kW/h)	−30
COP^{c}_{EC}	4	C_p/(kJ/(kg·°C))	1.5	R^M_{GB}/(kW/h)	48
η_{cha}	0.9	m/kg	20,000	R^m_{GB}/(kW/h)	−48
η_{dis}	0.9	P^M_{EB}/kW	50	R^M_{EB}/(kW/h)	15
$P^M_{ES,CH}$/kW	20	P^M_{EC}/kW	50	R^m_{EB}/(kW/h)	−15
$P^M_{ES,DIS}$/kW	20	E^M_{ES}/kWh	100	T^{ex}_{RF}, T^M_{RF}/°C	−18, −16
ξ_P/(¥/kWh)	6	E^M_{HS}/kWh	100	T^m_{tank}, T^{ex}_{tank}/°C	50, 65

Table 5. Parameters of devices in ISES.

Device	Failure Rate/(Times/a)	Repair Time/h
Gas input node	0.12	5
Power input node	0.15	5
CCHP	0.03	20
GT	0.03	20
GB	0.02	20
WT	0.02	10
PV	0.02	10
ES	0.03	20
HS	0.03	20
AC	0.02	20
EC	0.03	20

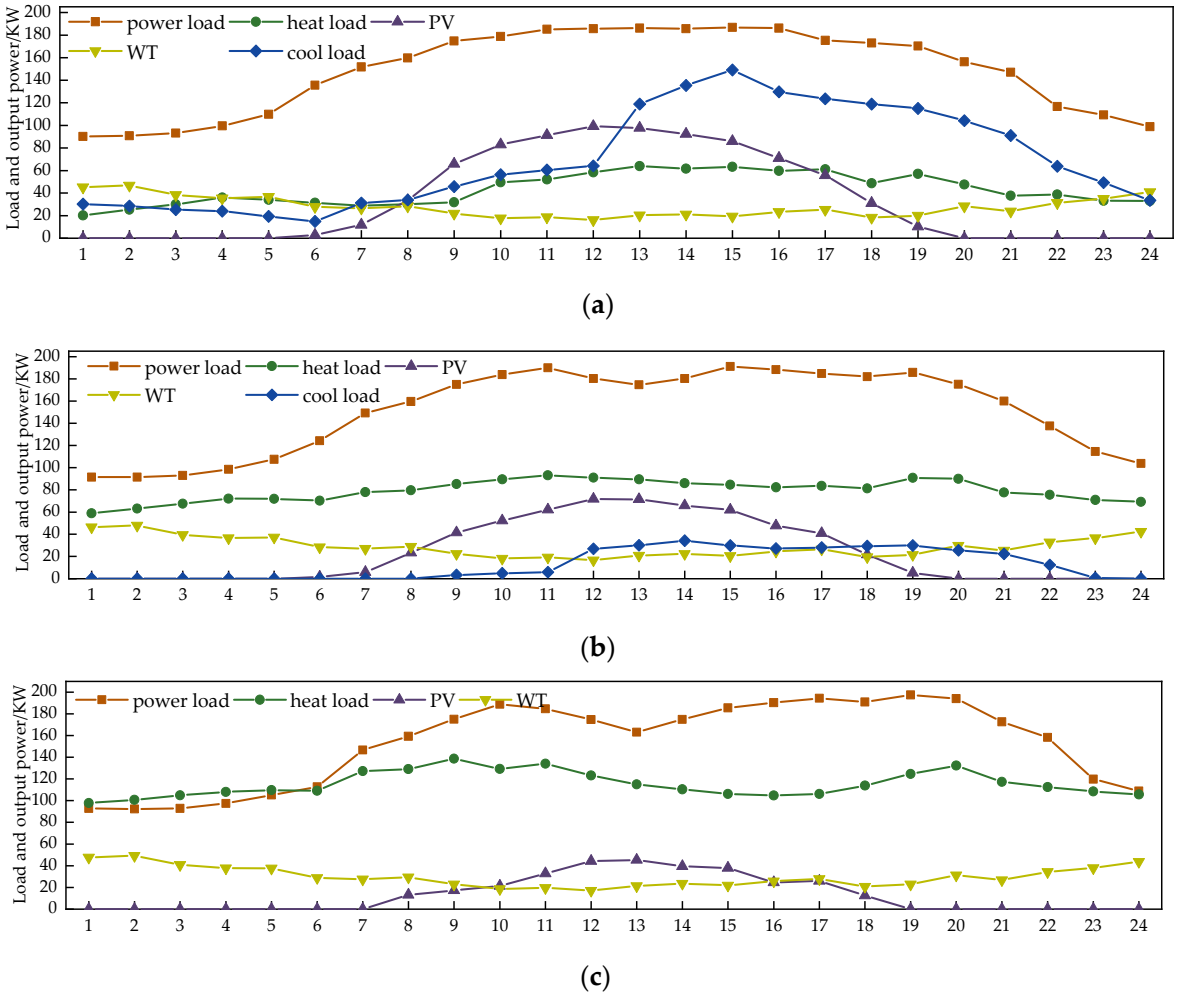

Figure 5. Predicted multi-energy loads of ISES and output of WT and PV. (**a**) Summer season typical day; (**b**) transitional season typical day; (**c**) winter season typical day.

5.2. The Impact of Thermal Inertia on the Reliability Assessment Results

Considering the occurrence of multiple load curtailments due to ISES failures, the impact of thermal inertia on the outputs of devices is analyzed in this section. Figure 6 shows the variations in curtailment indexes, the temperature of the hot tank and the heating output after the failure of the gas input node. The fault duration time $t_{TTR} = 16$ h from 6 a.m. to 9 p.m. A failure in the gas input node results in zero input power for the CCHP units, rendering them unable to output thermal power. The proposed two-stage scheduling

model dispatches the EB and HS to achieve maximum thermal power output. However, this adjustment still fails to meet the thermal load requirements, resulting in a curtailment in thermal load. From 6 a.m. to 2 p.m., considering the inertia of the hot water tank, the medium temperature remains within the permissible range, i.e., $T^{m}_{\mathrm{tan\,k}} \leq T^{t}_{\mathrm{tan\,k}} \leq T^{\mathrm{ex}}_{\mathrm{tan\,k}}$, leading to $x^{t}_{Qcut} = 0\,(t \in [6, 14])$. Then, from 3 p.m. to 9 p.m., the fault remains unresolved, and the thermal load curtailment continues. This led to the temperature of the hot water tank dropping below the lower limit $T^{m}_{\mathrm{tan\,k}}$, resulting in an interruption in the thermal load supply for the ISES.

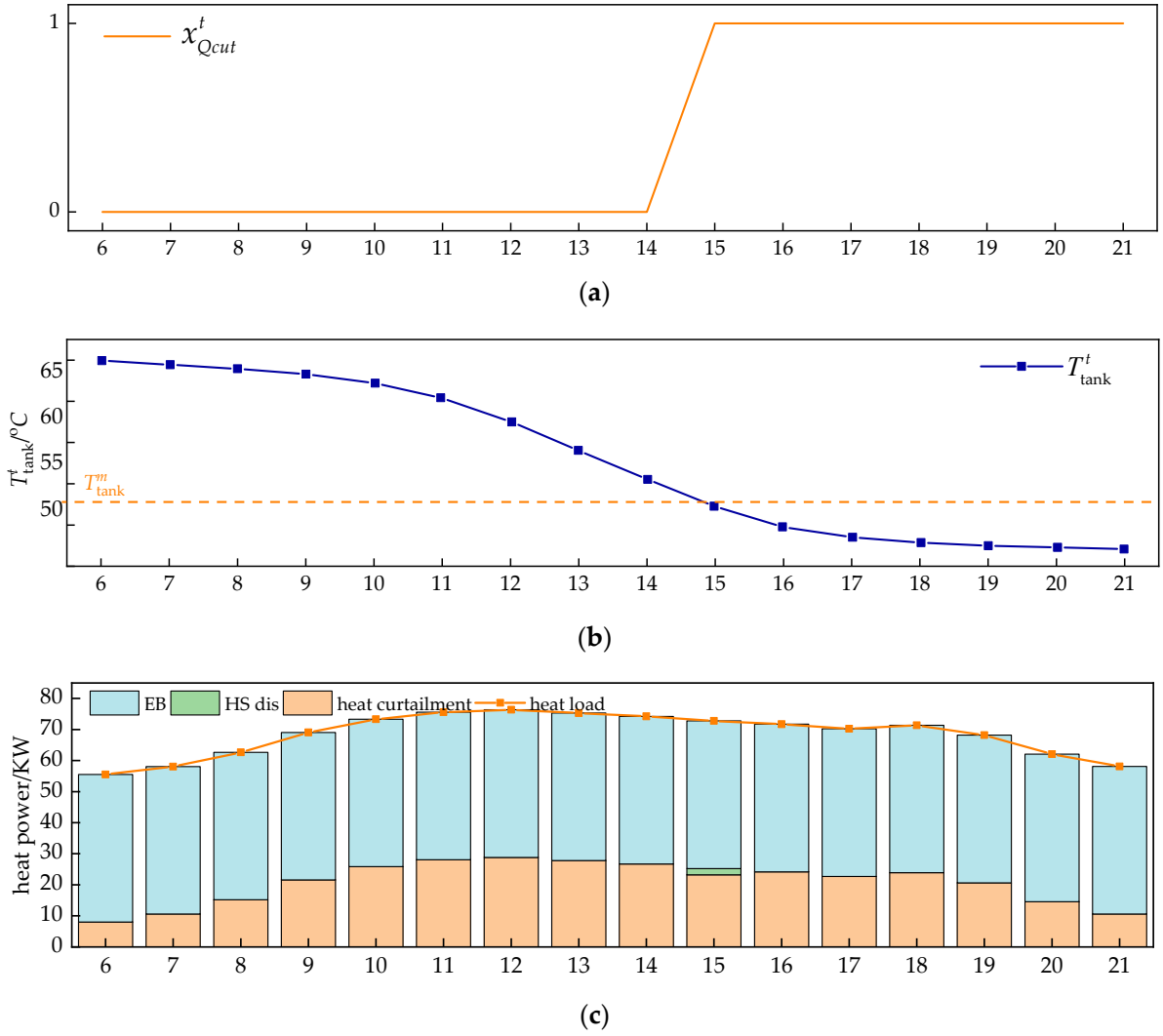

Figure 6. Variations in curtailment indexes, the temperature of the hot tank, and the heating output. (**a**) The curtailment indexes for the heating load; (**b**) the temperature curve of the hot water tank; (**c**) the heating output after two-stage optimization.

In summary, as illustrated in Figures 6 and 7, after a fault occurs, the temperatures of the hot water tank and RF remain within acceptable levels for a certain period, and the corresponding load curtailment can be excluded from the reliability index, which guarantees an accurate assessment of the reliability of the ISES.

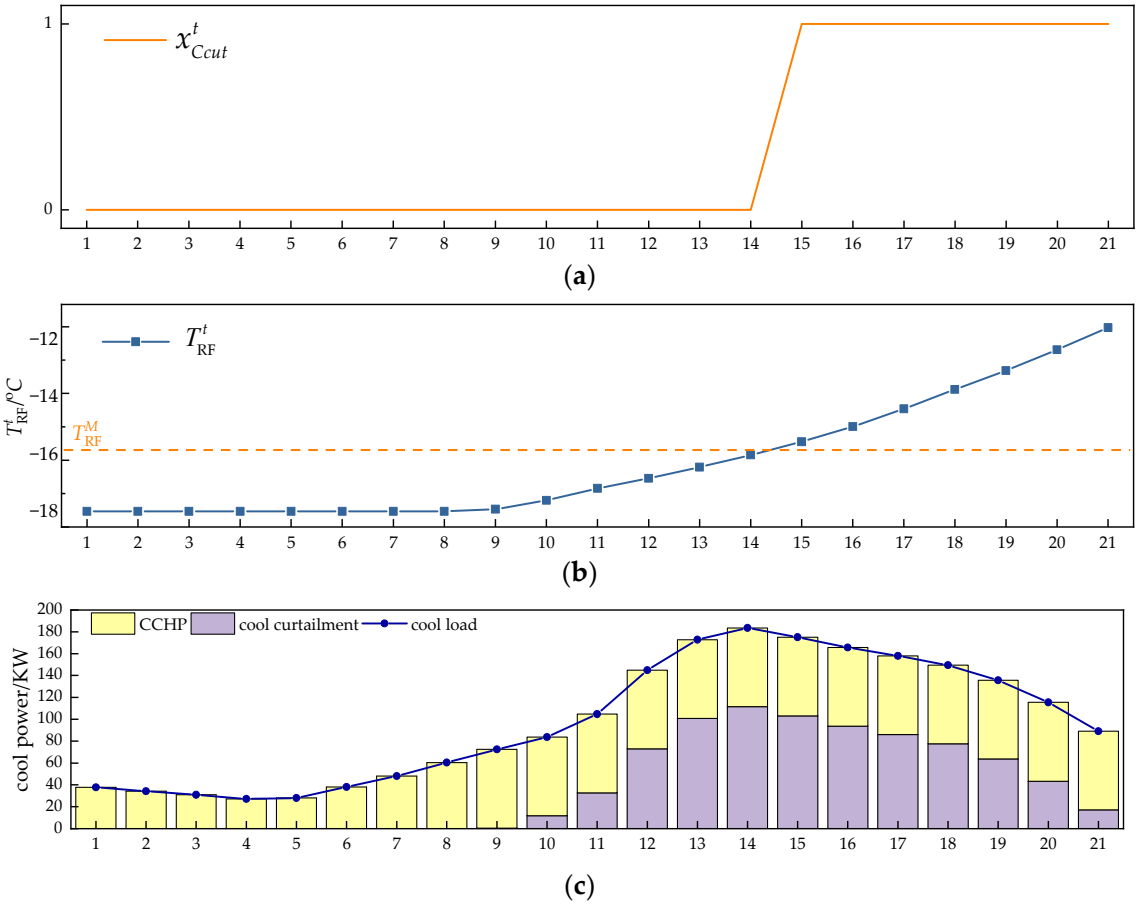

Figure 7. Variations in curtailment indexes, the temperature of RF, and the cooling output. (**a**) The curtailment indexes for cooling load; (**b**) the temperature curve of RF; (**c**) the cooling output after two-stage optimization.

Figure 7 shows the variations in curtailment indexes, the temperature of the RF, and the cooling output after the failure of EC, which lead to the cooling load curtailment during the fault duration time $t_{\mathrm{TTR}} = 21$ h, which is from 1 a.m. to 9 p.m. We can see that the temperature remained stable and that the CCHP can meet all the cooling loads within the first 9 h following the failure. Until the 10th hour, the cooling load demand of the ISES exceeds the maximum output of CCHP, resulting in an insufficient supply of cooling load. The temperature of the RF begins to rise. However, from 1 a.m. to 2 p.m., the temperature of the RF remained within the permissible range, i.e., $T^{\mathrm{ex}}_{\mathrm{RF}} \leq T^t_{\mathrm{RF}} \leq T^M_{\mathrm{RF}}$, leading to $x^t_{Ccut} = 0$ $(t \in [1, 14])$. After 3 p.m. to 9 p.m., insufficient cooling load supply caused the temperature of the RF to exceed the acceptable upper limit T^M_{RF}, resulting in an interruption in the thermal load supply for the ISES.

5.3. The Impact of Temperature Inertia on the ISES Reliability Indexes

This section compares three methods to verify the effectiveness of the proposed reliability assessment method during the fault period.

Method 1: According to [38], the output of the faulty component is adjusted to 0, and other components operate in the previous state before the fault.

Method 2: According to [24], the outputs of devices are adjusted based on the load curtailment method, which ignores the multiple thermal inertias.

Method 3: During the fault period, the outputs of devices are adjusted based on the proposed method, which considers the multiple thermal inertias.

Under the same conditions for other device parameters, the sequential Monte Carlo method is utilized to calculate the reliability indexes for the ISES, and the results are presented in Table 6.

Table 6. The reliability indexes of ISES using different methods.

Method	Electric Load		Heating Load		Cool Load		TSELE (¥/a)
	EENS (kWh/a)	LOLE (h/a)	EENS (kWh/a)	LOLE (h/a)	EENS (kWh/a)	LOLE (h/a)	
1	61.4118	0.7070	139.3543	3.6180	34.6448	1.6190	459.8669
2	57.8073	0.8590	26.3214	0.8020	2.4870	0.0700	225.4699
3	45.7438	0.7070	14.2229	0.2160	0.8549	0.0230	167.0491

Compared with Method 1, the EENS in the thermal load supply obtained by the proposed optimization model is diminished by 113.03 kWh/a, a relative reduction of 81.11%. The EENS in the cooling load is reduced by 32.16 kWh/a, a relative decrease of 92.82%. The LOLE for the heating load is 0.80 h/a, representing a decrease of 77.83%. The LOLE for cooling load curtailment is 0.07 h/a, corresponding to a relative reduction of 95.68%. Simultaneously, the TSELE is reduced by 234.34 CNY/a, representing a relative decrease of 50.97%. Since Method 1 ignores the energy interaction between different devices, the values of reliability indexes are poor. In fact, when the electrical load faces a risk of insufficient supply, CCHP increases the output to reduce the deficit in electrical load, while the EB and EC decrease the output to allocate more electrical energy for load supply. When the thermal load faces a risk of insufficient supply, CCHP, along with the GB, EB, and EC, increases the output to enhance the reliability of the thermal energy supply.

Additionally, compared with Method 2, after considering multiple thermal load inertia, the EENS in the electrical load supply is reduced by 12.06 kWh/a, corresponding to a relative decrease of 20.87%. The EENS in the thermal load supply further decreases by 12.09 kWh/a, representing a further reduction of 45.96%. The LOLE of the thermal load also reduces by 0.589 h/a, a relative decrease of 73.07%. The EENS in the cooling load decreases by 1.63 kWh/a in Method 2, a relative reduction of 65.63%. The LOLE of the cooling load also reduces by 0.05 h/a, a relative reduction of 67.14%. The TSELE decreases by 58.42 CNY/a, reflecting a relative reduction of 25.91%. The reason for this kind of result is that when the temperature of the hot water tank and RF remains within the permissible range, the insufficient energy supply does not affect the satisfaction of customers in the ISES. The value of x^t_{Qcut} and x^t_{Ccut} are set as 0, and the reliability indexes in (46), (48), and (49) decrease, which means that the heating and cooling reliability of the system is greatly improved.

6. Conclusions

This paper considers multiple thermal inertia in seaports and establishes a reliability assessment method based on sequential Monte Carlo simulation. The proposed two-stage optimal load curtailment model makes the ISES flexibly adjust the outputs of devices during the failure, significantly improving the energy supply reliability. After considering the thermal inertia, the expectation of energy not supply, the loss of load expectation, and the total shutdown energy loss expectation of the ISES are significantly reduced, which means that thermal inertia plays a positive role in the energy supply reliability of the ISES. The proposed Monte Carlo sequential-simulation-based reliability assessment method integrates the operational timing of all devices and effectively evaluates the reliability of the ISES energy supply.

With the increasing electrification level of equipment in seaport logistics, deep coupling exists between energy flow and logistics. Therefore, further research is needed to explore the impact of the coordinated scheduling of energy flow and logistics throughout the entire process on the reliability of the ISES.

Author Contributions: Conceptualization, T.Y. and Z.S.; methodology, T.Y.; software, Z.S.; validation, L.L.; formal analysis, Y.L.; investigation, T.Y.; resources, T.Y.; data curation, Z.S.; writing—original draft preparation, T.Y.; writing—review and editing, T.Y.; visualization, Z.S., L.L.; supervision, Y.L.; project administration, T.Y.; funding acquisition, T.Y. All authors have read and agreed to the published version of the manuscript.

Funding: This research was funded by the Basic Research Project of Liaoning Provincial Department of Education (LJKMZ20220363), the Fundamental Research Funds for the Central Universities (3132023113), and the China Postdoctoral Science Foundation (2021M700647).

Data Availability Statement: Data are contained within the article.

Conflicts of Interest: The authors declare no conflicts of interest. The funders had no role in the design of the study; in the collection, analyses, or interpretation of data; in the writing of the manuscript; or in the decision to publish the results.

References

1. Iris, Ç.; Lam, J.S.L. A review of energy efficiency in ports: Operational strategies, technologies and energy management systems. *Renew. Sustain. Energy Rev.* **2019**, *112*, 170–182. [CrossRef]
2. Xie, C.; Dehghanian, P.; Estebsari, A. Fueling the seaport of the future: Investments in low-carbon energy technologies for operational resilience in seaport multi-energy systems. *IET Gener. Transm. Distrib.* **2024**, *18*, 248–265. [CrossRef]
3. Wang, B.; Liu, Q.; Wang, L.; Chen, Y.; Wang, J. A review of the port carbon emission sources and related emission reduction technical measures. *Environ. Pollut.* **2023**, *320*, 121000. [CrossRef] [PubMed]
4. Zhang, Y.; Xiao, Y.; Shan, Q.; Li, T. Towards Lower Carbon Emissions: A Distributed Energy Management Strategy-Based Multi-Objective Optimization for the Seaport Integrated Energy System. *J. Mar. Sci. Eng.* **2023**, *3*, 681. [CrossRef]
5. Iris, Ç.; Lam, J.S. Optimal energy management and operations planning in seaports with smart grid while harnessing renewable energy under uncertainty. *Omega* **2021**, *103*, 102445. [CrossRef]
6. Teng, F.; Zhang, Q.; Xiao, G.; Ban, Z.; Liang, Y.; Guan, Y. Energy Management for a Port Integrated Energy System Based on Distributed Dual Decomposition Mixed Integer Linear Programming. *J. Mar. Sci. Eng.* **2023**, *11*, 1137. [CrossRef]
7. Mao, A.; Yu, T.; Ding, Z.; Fang, S.; Guo, J.; Sheng, Q. Optimal scheduling for seaport integrated energy system considering flexible berth allocation. *Appl. Energy* **2022**, *308*, 118386. [CrossRef]
8. Bui, V.D.; Nguyen, H.P.; Nguyen, X.P. Optimization of energy management systems in seaports as a potential strategy for sustainable development. *J. Mech. Eng. Res. Dev.* **2021**, *44*, 19–30.
9. Zhang, Y.; Wang, X.; He, J.; Xu, Y.; Pei, W. Optimization of distributed integrated multi-energy system considering industrial process based on energy hub. *J. Mod. Power Syst. Clean Energy* **2020**, *8*, 863–873. [CrossRef]
10. Kim, H.; Singh, C. Reliability modeling and simulation in power systems with aging characteristics. *IEEE Trans. Power Syst.* **2009**, *25*, 21–28.
11. Zhou, Y.; He, C. A review on reliability of integrated electricity-gas system. *Energies* **2022**, *15*, 6815. [CrossRef]
12. Zang, H.; Geng, M.; Huang, M.; Wei, Z.; Cheng, S.; Sun, G. Review and prospect of state estimation for electricity-heat-gas integrated energy system. *Autom. Electr. Power Syst.* **2022**, *46*, 187–199.
13. Lin, C.; Yuxiang, W.; Ning, Q. Review and prospect of research on operation reliability of power distribution and consumption system considering various distributed energy resources. *Autom. Electr. Power Syst.* **2021**, *45*, 191–207.
14. Ni, W.; Lv, L.; Xiang, Y.; Liu, J.; Huang, Y.; Wang, P. Reliability evaluation of integrated energy system based on Markov process Monte Carlo method. *Power Syst. Technol.* **2020**, *44*, 150–158.
15. Xu, B.; Sun, H.B.; Lu, G.; Zhang, Y. Maintenance optimization based on opportunistic maintenance for combined heat and power unit. *Electr. Power Constr.* **2018**, *39*, 88–94.
16. Kumar, S.; Saket, R.K.; Dheer, D.K.; Holm-Nielsen, J.B.; Sanjeevikumar, P. Reliability enhancement of electrical power system including impacts of renewable energy sources: A comprehensive review. *IET Gener. Transm. Distrib.* **2020**, *14*, 1799–1815. [CrossRef]
17. Liu, Y.; Su, Y.; Xiang, Y.; Liu, J.; Wang, L.; Xu, W. Operational reliability assessment for gas-electric integrated distribution feeders. *IEEE Trans. Smart Grid* **2018**, *10*, 1091–1100. [CrossRef]
18. Geidl, M.; Koeppel, G.; Favre-Perrod, P.; Klockl, B.; Andersson, G.; Frohlich, K. Energy hubs for the future. *IEEE Power Energy Mag.* **2006**, *5*, 24–30. [CrossRef]
19. Koeppel, G.; Andersson, G. Reliability modeling of multi-carrier energy systems. *Energy* **2009**, *34*, 235–244. [CrossRef]
20. Li, Z.; Wang, Z.; Fu, Y.; Zhao, N. Energy supply reliability assessment of the integrated energy system considering complementary and optimal operation during failure. *IET Gener. Transm. Distrib.* **2021**, *15*, 1897–1907. [CrossRef]
21. Xianjun, Q.; Qiao, C.; Hongbin, W. Impact of incentive-based demand response on operational reliability of distribution network. *Trans. China Electrotech. Soc.* **2018**, *33*, 5319–5326.
22. Fang, J.; Zeng, Q.; Ai, X.; Chen, Z.; Wen, J. Dynamic optimal energy flow in the integrated natural gas and electrical power systems. *IEEE Trans. Sustain. Energy* **2017**, *9*, 188–198. [CrossRef]

23. Yao, S.; Gu, W.; Lu, S.; Zhou, S.; Wu, Z.; Pan, G.; He, D. Dynamic optimal energy flow in the heat and electricity integrated energy system. *IEEE Trans. Sustain. Energy* **2020**, *12*, 179–190. [CrossRef]
24. Liu, W.; Wang, Y.; Shi, Q.; Wan, H.; Fu, M. Optimization of decentralized control strategies of distributed resources under cyber failures in flexible distribution network. *Int. J. Electr. Power Energy Syst.* **2022**, *142*, 108320. [CrossRef]
25. Zhang, S.; Wen, M.; Cheng, H.; Hu, X.; Xu, G. Reliability evaluation of electricity-heat integrated energy system with heat pump. *CSEE J. Power Energy Syst.* **2018**, *4*, 425–433. [CrossRef]
26. Liu, W.; Ma, T.; Yang, Y. A Reliability assessment of an integrated energy system based on coupling energy flow and thermal inertia. *CSEE J. Power Energy Syst.* **2020**, *8*, 1772–1783.
27. Wang, S.; Shao, C.; Ding, Y.; Yan, J. Operational reliability of multi-energy customers considering service-based self-scheduling. *Appl. Energy* **2019**, *254*, 113531. [CrossRef]
28. Cao, M.; Shao, C.; Hu, B.; Xie, K.; Li, W.; Peng, L.; Zhang, W. Reliability assessment of integrated energy systems considering emergency dispatch based on dynamic optimal energy flow. *IEEE Trans. Sustain. Energy* **2021**, *13*, 290–301. [CrossRef]
29. Li, M.; Mu, H.; Li, N.; Ma, B. Optimal design and operation strategy for integrated assessment of CCHP (combined cooling heating and power) system. *Energy* **2016**, *99*, 202–220. [CrossRef]
30. Shi, Z.; Fan, F.; Tai, N.; Qing, C.; Meng, Y.; Guo, R. An Optimal Operation Strategy for Integrated Energy-Logistics System in Green Port. In Proceedings of the 2022 IEEE/IAS Industrial and Commercial Power System Asia, Shanghai, China, 8–11 July 2022; pp. 1592–1597.
31. Gennitsaris, S.G.; Kanellos, F.D. Kanellos. Emission-aware and cost-effective distributed demand response system for extensively electrified large ports. *IEEE Trans. Power Syst.* **2019**, *6*, 4341–4351. [CrossRef]
32. Yanyan, C.; Wei, L.; Jian, S. Reliability assessment of integrated energy system considering optimal load reduction and thermal load inertia. *Electr. Power Constr.* **2021**, *42*, 40–48.
33. Fan, F.; Aditya, V.; Xu, Y.; Cheong, B.; Gupta, A.K. Robustly coordinated operation of a ship microgrid with hybrid propulsion systems and hydrogen fuel cells. *Appl. Energy* **2022**, *312*, 118738. [CrossRef]
34. Fang, L.B.; Cai, J.D. Reliability assessment of microgrid using Monte Carlo sequential simulation. *J. Electron. Sci. Technol.* **2011**, *9*, 31–34.
35. Liu, W.; Guo, D.; Xu, Y.; Cheng, R.; Wang, Z.; Li, Y. Reliability assessment of power systems with photovoltaic power stations based on intelligent state space reduction and pseudo-Monte Carlo sequential simulation. *Energies* **2018**, *11*, 1431. [CrossRef]
36. Song, T.; Li, Y.; Zhang, X.P.; Wu, C.; Li, J.; Guo, Y.; Gu, H. Integrated port energy system considering integrated demand response and energy interconnection. *Int. J. Electr. Power Energy Syst.* **2020**, *117*, 105654. [CrossRef]
37. Gu, W.; Wang, J.; Lu, S.; Luo, Z.; Wu, C. Optimal operation for integrated energy system considering thermal inertia of district heating network and buildings. *Appl. Energy* **2017**, *199*, 234–246. [CrossRef]
38. Zhang, X.; Li, J.; Zhang, L.; Wu, B.; Wang, L.; Tang, W. Integrated energy system planning considering peak-to-valley difference of tie line and operation benefit of power grid. *Electr. Power Autom. Equip.* **2019**, *39*, 195–202.